

Spatial correlations of Rydberg excitations in optically driven atomic ensembles

David Petrosyan,¹ Michael Höning,² and Michael Fleischhauer²

¹*Institute of Electronic Structure and Laser, FORTH, GR-71110 Heraklion, Crete, Greece*

²*Fachbereich Physik und Forschungszentrum OPTIMAS,
Technische Universität Kaiserslautern, D-67663 Kaiserslautern, Germany*

(Dated: July 5, 2018)

We study the emergence of many-body correlations in the stationary state of continuously-driven, strongly-interacting dissipative system. Specifically, we examine resonant optical excitations of Rydberg states of atoms interacting via long-range dipole-dipole and van der Waals potentials employing exact numerical solutions of the density matrix equations and Monte-Carlo simulations. Collection of atoms within a blockade distance form a “superatom” that can accommodate at most one Rydberg excitation. The superatom excitation probability saturates to $\frac{1}{2}$ for coherently driven atoms, but is significantly higher for incoherent driving, approaching unity as the number of atoms increases. In the steady state of uniformly-driven, extended one-dimensional system, the saturation of superatoms leads to quasi-crystallization of Rydberg excitations whose correlations exhibit damped spatial oscillations. The behavior of the system under the van der Waals interaction potential can be approximated by an analytically soluble model based on a “hard-rod” interatomic potential.

PACS numbers: 32.80.Ee, 32.80.Rm, 71.10.Pm, 42.50.Gy,

I. INTRODUCTION

Strong, long-range dipole-dipole (DD) or van der Waals (vdW) interactions between atoms in highly excited Rydberg states [1] can suppress multiple Rydberg excitations within a certain interaction (blockade) volume, while enhancing the rate of single collective excitation [2–8]. The resulting dipole blockade constitutes the basis for a number of promising quantum information schemes [9] and interesting many-body effects involving long-range correlations and crystallization of Rydberg excitations [10–27].

Much of the research on strongly interacting Rydberg atoms is focused on the unitary dynamics or eigenstates of the many-body system. In coherently driven ensembles of atoms, depending on the strength and detuning of driving lasers, different ground-state phases with crystalline order emerge [10–15]. Yet, adiabatically attaining the ground state of a large system requires exceeding preparation times [16, 17] during which the decoherence and dissipation associated with the optical excitation cannot be neglected. This necessitates the consideration of open systems and their stationary states [27], which is the main purpose of this paper.

We study theoretically resonant optical excitations of Rydberg states of atoms interacting with each other via DD and vdW potentials. Atoms within a blockade distance form a “superatom” which can accommodate at most one collective Rydberg excitation [2, 8, 28–30]. We show that the steady-state excitation probability of the superatom saturates to $\frac{1}{2}$ for coherently driven atoms, but can be significantly higher in the presence of strong dephasing which suppresses inter-atomic coherences and disentangles the atoms [30]. This case is amenable to an iterative Monte-Carlo sampling algorithm which can accurately and efficiently simulate the stationary state of the many-body system. We apply this algorithm to

extended one-dimensional (1D) atomic ensembles, and explore both the low-density (lattice) regime [24, 27] with one or few atoms per blockade distance, and the high-density (continuous) regime [23] with many atoms per blockade distance. For the vdW interacting atoms at high densities, tight packing of superatoms leads to quasi-crystallization of Rydberg excitations, similar to the predictions of an analytic model involving a “hard-rod” (HR) interatomic potential [21]. In contrast, the DD potential appears to be too “soft” for assigning a well-defined interaction range at high atomic densities.

The paper is organized as follows. In Sec. II we introduce the Hamiltonian and dissipative terms of the master equation for the density matrix of the many-body system and examine the properties of superatoms under coherent and incoherent driving. In Sec. III we study extended 1D systems, employing exact solution of the density matrix equations for several atoms, and Monte Carlo simulations for hundreds of atoms. A model based on the HR interatomic potential is analytically solved in Sec. IV and compared with the results of numerical simulations for the vdW interacting atoms. Experimental considerations and conclusions are summarized in Sec. V

II. THE MANY-BODY SYSTEM

We consider an ensemble of N atoms irradiated by a uniform driving field that couples near-resonantly the atomic ground state $|g\rangle$ to the highly excited Rydberg state $|r\rangle$ with Rabi frequency Ω , Fig. 1(a). A pair of atoms i and j at positions \mathbf{x}_i and \mathbf{x}_j excited to states $|r\rangle$ interact either via the DD ($p = 3$) [31] or vdW ($p = 6$) [32] potential $\hbar\Delta(\mathbf{x}_i - \mathbf{x}_j) = \hbar C_p |\mathbf{x}_i - \mathbf{x}_j|^{-p}$. In the frame rotating with the driving field frequency ω , the system Hamiltonian $\mathcal{H} = \mathcal{V}_{af} + \mathcal{V}_{aa}$ is composed of the atom-field and atom-atom interactions, $\mathcal{V}_{af} = -\hbar \sum_j^N [\delta \hat{\sigma}_{rr}^j +$

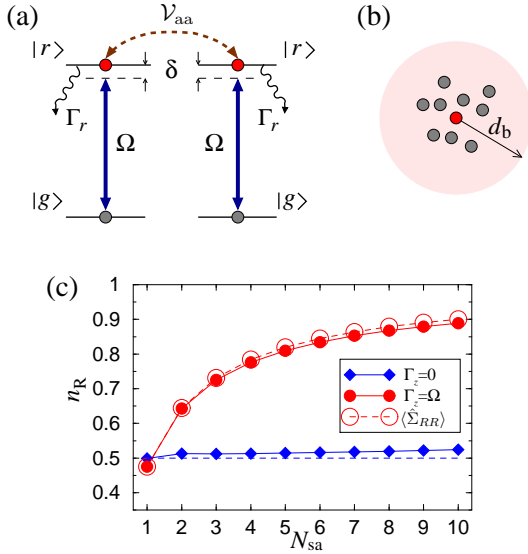


FIG. 1. (a) Level scheme of atoms interacting with the driving field Ω on transition $|g\rangle \rightarrow |r\rangle$ with detuning δ , while \mathcal{V}_{aa} denotes the DD or vdW interaction between the atoms in Rydberg state $|r\rangle$ having the (population) decay rate Γ_r . (b) Atoms within the blockade distance d_b form a superatom with at most one Rydberg excitation. (c) Mean number of Rydberg excitations n_R of superatom containing $N_{sa} \leq 10$ atoms within $L = 0.7d_b$ (vdW interaction), obtained from the exact steady-state solutions of Eq. (1) for $\delta = 0$, $\Gamma_r = 0.1\Omega$, and $\Gamma_z = 0$ (filled blue diamonds) and $\Gamma_z = \Omega$ (filled red circles). Also shown the Rydberg excitation probability $\langle \hat{\Sigma}_{RR} \rangle$ of superatom (empty red circles) as per Eq. (4).

$\Omega(\hat{\sigma}_{rg}^j + \hat{\sigma}_{gr}^j)$ and $\mathcal{V}_{aa} = \hbar \sum_{i < j}^N \hat{\sigma}_{rr}^i \Delta(\mathbf{x}_i - \mathbf{x}_j) \hat{\sigma}_{rr}^j$, where $\hat{\sigma}_{\mu\nu}^j \equiv |\mu\rangle_{jj}\langle\nu|$ is the transition ($\mu \neq \nu$) or projection ($\mu = \nu$) operator for atom j at position \mathbf{x}_j , and $\delta = \omega - \omega_{rg}$ is the driving field detuning. The relaxation processes affecting the atoms include the spontaneous (radiative) decay of the excited state $|r\rangle$ with rate Γ_r , and the (non-radiative) dephasing of atomic coherence $\hat{\sigma}_{rg}$ with rate Γ_z ; the decay rate of the Rydberg state is typically small compared to Ω , while the physical origins of dephasing include non-radiative collisions, Doppler shifts or the excitation laser linewidth. The decay and dephasing Liouvillians, acting independently on each atom, are given, respectively, by $\mathcal{L}_r^j \hat{\rho} = \frac{1}{2} \Gamma_r [2\hat{\sigma}_{gr}^j \hat{\rho} \hat{\sigma}_{rg}^j - \hat{\sigma}_{gg}^j \hat{\rho} - \hat{\rho} \hat{\sigma}_{gg}^j]$ and $\mathcal{L}_z^j \hat{\rho} = \Gamma_z [(\hat{\sigma}_{rr}^j - \hat{\sigma}_{gg}^j) \hat{\rho} (\hat{\sigma}_{rr}^j - \hat{\sigma}_{gg}^j) - \hat{\rho}]$ [33]. The density matrix $\hat{\rho}$ of the N -atom system obeys the master equation

$$\partial_t \hat{\rho} = -\frac{i}{\hbar} [\mathcal{H}, \hat{\rho}] + \mathcal{L} \hat{\rho}, \quad (1)$$

with $\mathcal{L} \hat{\rho} = \sum_j^N (\mathcal{L}_r^j \hat{\rho} + \mathcal{L}_z^j \hat{\rho})$.

A. Blockade distance

For a single two-level atom, the steady-state population of the excited state $|r\rangle$ is a Lorentzian function of

detuning δ ,

$$\langle \hat{\sigma}_{rr} \rangle = \frac{\Omega^2}{2\Omega^2 + \frac{\Gamma_r}{2\gamma_{rg}}(\gamma_{rg}^2 + \delta^2)}, \quad (2)$$

with the width $w = \gamma_{rg} \sqrt{4\Omega^2 / \Gamma_r \gamma_{rg} + 1}$, where $\gamma_{rg} \equiv \frac{1}{2}\Gamma_r + 2\Gamma_z$ is the total (transversal) relaxation rate of the $\hat{\sigma}_{rg}$ coherence [33]. For strong ($\Omega^2 > \Gamma_r \gamma_{rg}$) resonant ($\delta \ll w$) driving, the population saturates to $\langle \hat{\sigma}_{rr} \rangle \rightarrow \frac{1}{2}$. But given an atom in the Rydberg state $|r\rangle$, it will induce a level shift Δ —equivalent to detuning δ —of another atom, blocking its Rydberg excitation when $\Delta \gtrsim w$. We may therefore define the blockade distance d_b via $\Delta(d_b) = w$, which yields

$$d_b \equiv \sqrt[p]{\frac{C_p}{w}} \simeq \left(\frac{C_p}{2\Omega} \sqrt{\frac{\Gamma_r}{\gamma_{rg}}} \right)^{1/p}, \quad (3)$$

with $p = 3$ for the DD interaction and $p = 6$ for the vdW interaction.

B. The superatom

Consider N_{sa} atoms within distance $L < d_b$, such that $\Delta(\mathbf{x}_i - \mathbf{x}_j) \gg w$ for any pair of atoms i and j , Fig. 1(b). We thus expect that the “superatom” can accommodate at most one Rydberg excitation [28, 29]. This is confirmed by our exact numerical simulations for $N_{sa} \leq 10$; starting with all the atoms in the ground state $|g\rangle$, we propagate Eq. (1) for time $t (\gg \Omega^{-1})$ long enough until the steady-state is reached. In Fig. 1(c) we show the resulting mean number of Rydberg excitations $n_R = \langle \sum_j^{N_{sa}} \hat{\sigma}_{rr}^j \rangle$ within the superatom. Clearly, $n_R < 1 \forall N_{sa}$, while we verify that the probabilities of double $\langle \hat{\sigma}_{rr}^i \hat{\sigma}_{rr}^j \rangle$, triple $\langle \hat{\sigma}_{rr}^i \hat{\sigma}_{rr}^j \hat{\sigma}_{rr}^k \rangle$, etc. excitations are always small.

In the absence of dephasing, $\Gamma_z = 0$ and $\gamma_{rg} = \frac{1}{2}\Gamma_r \ll \Omega$, we have $n_R \simeq \frac{1}{2}$ independent of N_{sa} . The ground state $|G\rangle = |g_1, g_2, \dots, g_{N_{sa}}\rangle$ of the superatom is coupled only to the single collective Rydberg excitation state $|R^{(1)}\rangle = \frac{1}{\sqrt{N_{sa}}} \sum_j^{N_{sa}} |g_1, g_2, \dots, r_j, \dots, g_{N_{sa}}\rangle$, while all the states $|R^{(n)}\rangle$ with higher number $n > 1$ of Rydberg excitations are shifted out of resonance by the strong interatomic interaction \mathcal{V}_{aa} and therefore are not populated. As the collective Rabi frequency $\sqrt{N_{sa}}\Omega$ saturates the transition $|G\rangle \leftrightarrow |R^{(1)}\rangle$, the superatom ground and excited states acquire populations $\langle \hat{\Sigma}_{GG} \rangle \simeq \langle \hat{\Sigma}_{RR} \rangle \simeq \frac{1}{2}$, where $\hat{\Sigma}_{GG} \equiv \prod_{j=1}^{N_{sa}} \hat{\sigma}_{gg}^j$ and $\hat{\Sigma}_{RR} \equiv \sum_{j=1}^{N_{sa}} \hat{\sigma}_{rr}^j \prod_{i \neq j}^{N_{sa}} \hat{\sigma}_{gg}^i$ are projectors onto the ground and single Rydberg excitation states of N_{sa} atoms. We note that n_R slightly larger than $\frac{1}{2}$ seen in Fig. 1(c) is due to imperfect blockade of Rydberg excitation [$\Delta(L) \sim 10w$] of atoms at the boundaries of the region of finite size [$L = 0.7d_b$].

Remarkably, strong dephasing Γ_z increases the mean number of Rydberg excitations $n_R > \frac{1}{2}$ within the superatom. The transversal relaxation $\gamma_{rg} \gtrsim \Omega$ destroys

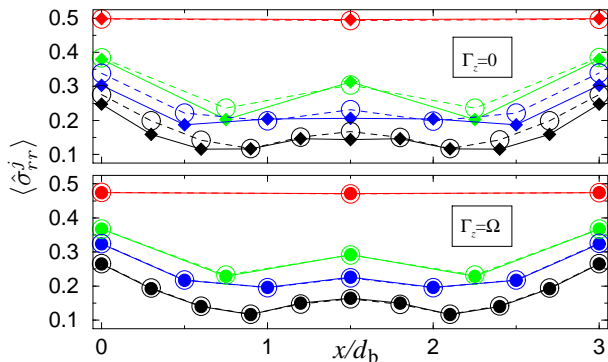


FIG. 2. Rydberg state populations $\langle \hat{\sigma}_{rr}^j \rangle$ of $N = 3, 5, 7, 11$ atoms (from top to bottom: red, green, blue, black) in a 1D lattice of length $L = 3d_b$ (vdW interaction) obtained from the exact solutions of Eq. (1) for $\delta = 0$, $\Gamma_r = 0.1\Omega$, and $\Gamma_z = 0$ (upper panel) and $\Gamma_z = \Omega$ (lower panel). Also shown the corresponding Rydberg excitation probabilities $\bar{\sigma}_{rr}^j$ (empty circles) obtained from MC simulations.

the inter- and intra-atomic coherences, causing individual atoms to behave independently. In the basis of collective, singly-excited states, this corresponds to a coupling of the symmetric state $|R^{(1)}\rangle$ to all the non-symmetric states [30]. The superatom still contains at most one Rydberg excitation, $\hat{\Sigma}_{GG} + \hat{\Sigma}_{RR} = \mathbb{1}$, which, upon combining with $\hat{\sigma}_{gg}^j + \hat{\sigma}_{rr}^j = \mathbb{1}$, yields

$$\langle \hat{\Sigma}_{RR} \rangle = \frac{N_{\text{sa}} \langle \hat{\sigma}_{rr} \rangle}{(N_{\text{sa}} - 1) \langle \hat{\sigma}_{rr} \rangle + 1}, \quad (4)$$

where $\langle \hat{\sigma}_{rr} \rangle$ is given by Eq. (2). For $N_{\text{sa}} = 1$ we have $\langle \hat{\Sigma}_{RR} \rangle = \langle \hat{\sigma}_{rr} \rangle$ as it should, while $N_{\text{sa}} \gg 1/\langle \hat{\sigma}_{rr} \rangle$ leads to $\langle \hat{\Sigma}_{RR} \rangle \rightarrow 1$. In Fig. 1(c) we plot $\langle \hat{\Sigma}_{RR} \rangle$, which reproduces well the exact numerical solution, $n_R \simeq \langle \hat{\Sigma}_{RR} \rangle$, under the same conditions.

III. EXTENDED 1D SYSTEM

We next consider the steady-state distribution of Rydberg excitations in a 1D system of $N = \rho_{\text{at}}L$ atoms of linear density ρ_{at} .

A. Small system

We have performed exact numerical simulations of the density matrix Eqs. (1) for $N \leq 11$ atoms with and without dephasing Γ_z . In Fig. 2 we show the stationary populations $\langle \hat{\sigma}_{rr}^j \rangle$ of Rydberg states of vdW interacting atoms in a lattice of length $L = 3d_b$ [open boundary conditions (OBC)]. When the interatomic distance exceeds d_b ($N = 3$), interactions play no role and the population $\langle \hat{\sigma}_{rr}^j \rangle$ for each atom is given by Eq. (2). With increasing atomic density, interactions progressively suppress the Rydberg state populations of individual atoms.

Simultaneously, we observe an onset of spatial oscillations of Rydberg excitations $\langle \hat{\sigma}_{rr}^j \rangle$. Note that at higher atomic densities ($N \geq 7$), the oscillations are somewhat smoother and more pronounced in the presence of strong dephasing $\gamma_{rg} \gtrsim \Omega$.

B. Monte-Carlo algorithm

The dephasing suppresses interatomic coherences and disentangles the atoms, admitting only classical N -body correlations. Each atom then behaves as a driven two-level system of Eq. (2) but with the detuning δ determined by operator $\hat{S}_j \equiv \sum_{i \neq j}^N \hat{\sigma}_{rr}^i \Delta(\mathbf{x}_i - \mathbf{x}_j)$ which describes the total interaction-induced shift of level $|r\rangle$ for an atom at position \mathbf{x}_j involving the contributions of all the Rydberg atoms $\hat{\sigma}_{rr}^i$ at positions \mathbf{x}_i .

We can now introduce an efficient procedure to simulate the stationary distribution of Rydberg excitation probabilities at any atomic density ρ_{at} . Our algorithm relies on iterative Monte-Carlo (MC) sampling of $\{\hat{\sigma}_{rr}^j\}$ for an ensemble of N atoms, in the spirit of the Hartree-Fock method. We start with, e.g., all the atoms in the ground state, $\langle \hat{\sigma}_{gg}^j \rangle = 1 \forall j \in [1, N]$, although the resulting steady-state does not depend on the initial configuration. At every step, for each atom j , we draw a uniform random number $s \in [0, 1]$ and compare it with the Rydberg state population $\langle \hat{\sigma}_{rr}^j \rangle$; if $s \leq \langle \hat{\sigma}_{rr}^j \rangle$, we set $\hat{\sigma}_{rr}^j \rightarrow 1$, otherwise $\hat{\sigma}_{rr}^j \rightarrow 0$. In turn, the thus constructed binary configuration of Rydberg excitations $\{\hat{\sigma}_{rr}^i\} \rightarrow \{0, 1, 0, 0, \dots\}$ determines the level shift \hat{S}_j (equivalent to detuning δ) of atom j when evaluating $\langle \hat{\sigma}_{rr}^j \rangle$. We continuously iterate this procedure, sifting repeatedly through every atom in the potential generated by all the other atoms, in the self consistent way. The probability distribution $\bar{\sigma}_{rr}^j$ of Rydberg excitations results from averaging over many ($\sim 10^6$) configurations $\{\hat{\sigma}_{rr}^j\}$. We note a related algorithm employed in [34]. In Fig. 2 we plot $\bar{\sigma}_{rr}^j$ for various N and verify that, for strong dephasing ($\Gamma_z = \Omega$), the algorithm accurately reproduces the exact steady-state populations $\langle \hat{\sigma}_{rr}^j \rangle$. In the absence of dephasing ($\Gamma_z = 0$), however, the steady-state resulting from the MC simulations quantitatively differs from the exact state of the system.

C. Large system

We employ the above MC procedure to study realistically large 1D systems of up to $N \sim 10^3$ atoms interacting via the DD and vdW interactions and subject to strong dephasing. In Fig. 3(a) we show the spatial distribution of Rydberg excitation probabilities in a finite system of length $L = 15d_b$ (OBC) for different atomic densities. Interactions between the atoms suppress the Rydberg excitation probabilities $\bar{\sigma}_{rr}^j$, the more the higher is the atomic density (smaller the interatomic distance) and stronger

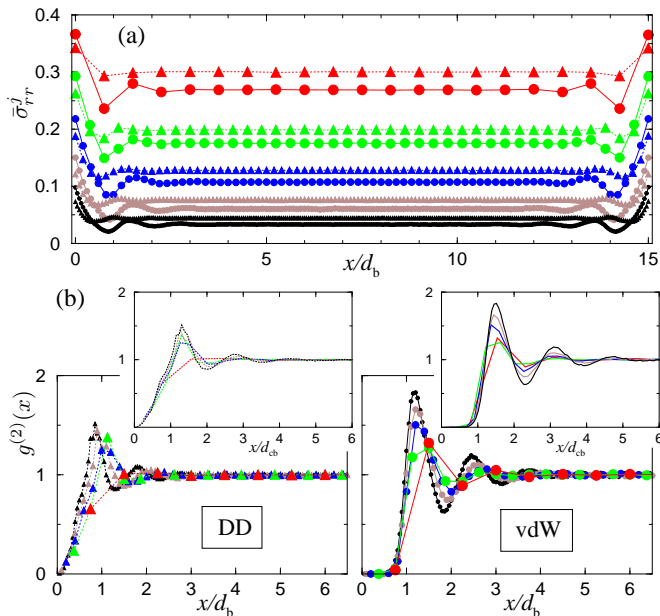


FIG. 3. (a) Probabilities $\bar{\sigma}_{rr}^j$ of Rydberg excitations in a 1D atomic ensemble of length $L = 15d_b$ (OBC) obtained from MC simulations with $\delta = 0$, $\Gamma_r = 0.1\Omega$, and $\Gamma_z = \Omega$. Triangles (connected by dotted lines) correspond to the DD interaction, and circles (connected by solid lines) to the vdW interaction between the atoms. The atomic densities are, from top to bottom: $\rho_{at}d_b = 1\frac{1}{3}, 2\frac{2}{3}, 5, 10, 20$ (red, green, blue, brown, black). (b) The corresponding 1D spatial correlations $g^{(2)}(x)$ of Rydberg excitations of DD (left) and vdW (right) interacting atoms. In the inset of each graph, $g^{(2)}(x)$ is plotted versus x in units of the corresponding collective blockade distance d_{cb} of Eq. (5).

the interaction. The Rydberg excitations are then repelled to the boundaries of the system. An atom at the edge, having higher probability to be excited, suppresses the excitation of the neighboring atoms within the blockade distance, beyond which another atom acquires higher excitation probability. Hence a Rydberg excitation density wave develops. This behavior is significantly more pronounced for the vdW interaction between the atoms, which is stronger within the blockade distance but falls off fast outside of it, as compared to the DD interaction, which is weaker at short distances and has longer tails. The vdW potential is thus more reminiscent of a “hard-rod” interaction, while the DD potential is much “softer”.

From many configurations $\{\hat{\sigma}_{rr}^j\}$, we can extract the spatial correlations of Rydberg excitations $G^{(2)}(x \equiv |\mathbf{x}_i - \mathbf{x}_j|) = \overline{\hat{\sigma}_{rr}^i \hat{\sigma}_{rr}^j}$. More explicitly, we place a Rydberg atom ($\hat{\sigma}_{rr}^i = 1$) at the origin $\mathbf{x}_i = 0$, and then use the above MC procedure to calculate $\bar{\sigma}_{rr}^j \forall \mathbf{x}_j > 0$, from which we obtain the normalized correlation function as $g^{(2)}(x) = \bar{\sigma}_{rr}^j / \bar{\sigma}_{rr}$, where $\bar{\sigma}_{rr} = \frac{1}{N} \sum_{j=1}^N \bar{\sigma}_{rr}^j$ is the spatial average with $N \gg 1$ ($L \gg d_b$). In Fig. 3(b) we show the corresponding $g^{(2)}(x)$ for the DD and vdW interactions. In the case of vdW interaction, the Rydberg atom at $x = 0$ almost

completely blocks the excitation of all the atoms within the blockade distance $x \lesssim d_b$. In contrast, for the DD potential the excitation blockage is only partial as $g^{(2)}(x)$ grows nearly linearly in the region of $x < d_b$. In addition, for higher atomic densities $\rho_{at}d_b > 5$, we observe damped spatial oscillations of $g^{(2)}(x)$ with increasing amplitude and slowly decreasing period λ close to d_b .

D. Collective blockade distance

In a dense system, $\rho_{at}d_b \gg 1$, an atom in the Rydberg state $|r\rangle$ blocks the excitation of other atoms within a certain distance which, due to collective effects, is somewhat smaller than the blockade distance d_b for a pair of atoms, Eq. (3). To estimate the collective blockade distance d_{cb} , note that the collective Rabi frequency $\Omega_{cb} = \sqrt{N_{cb}}\Omega$, and thereby the excitation linewidth $w_{cb} \simeq 2\Omega_{cb}\sqrt{\gamma_{rg}/\Gamma_r}$ for $N_{cb} = \rho_{at}d_{cb}$ atoms is enhanced by a factor of $\sqrt{N_{cb}}$. Substituting N_{cb} into the definition of $d_{cb} \equiv \sqrt[3]{C_p/w_{cb}}$ yields

$$d_{cb} = \left(\frac{C_p}{\sqrt{\rho_{at}w}} \right)^{2/(2p+1)} = \frac{d_b}{(\rho_{at}d_b)^{1/(2p+1)}}, \quad (5)$$

with $p = 3$ for DD and $p = 6$ for vdW interactions. In turn, the number of atoms within the collective blockade distance is $N_{cb} = (\rho_{at}d_b)^{2p/(2p+1)}$.

In the insets of Fig. 3(b) we plot the correlation functions $g^{(2)}(x)$ with x rescaled by the corresponding (density-dependent) collective blockade distance d_{cb} . For vdW interaction, all the curves for different atomic densities then exhibit the same oscillation period $\lambda \simeq 1.75d_{cb}$.

The average (background) density of Rydberg excitations $\bar{\rho}_{vdW} = \rho_{at}\bar{\sigma}_{rr}$ can also be deduced from the collective excitation picture. For the average probability of the Rydberg state of vdW interacting atoms we obtain

$$\bar{\sigma}_{rr} \approx \frac{\langle \hat{\Sigma}_{RR} \rangle}{N_{sa}} = \frac{\langle \hat{\sigma}_{rr} \rangle}{(N_{sa} - 1)\langle \hat{\sigma}_{rr} \rangle + 1}, \quad (6)$$

where $N_{sa} \approx 1.83(\rho_{at}d_b)^{12/13} \sim 2N_{cb}$ is the effective number of atoms per superatom [see Fig. 4(a)]. Note that superatoms overlap.

IV. HARD-ROD POTENTIAL MODEL

We have seen above that the vdW interaction between the atoms in Rydberg states results in almost complete blockade of simultaneous excitation of two or more atoms within a distance close to d_b . This suggests an analogy between the vdW interaction potential and a HR potential of a range $d_r \sim d_b$ [21]. The model of incoherently driven atoms interacting via the HR potential admits an analytic solution presented below. Our aim is quantitative comparison of its predictions with the result of numerical simulations for vdW interacting atoms at high densities.

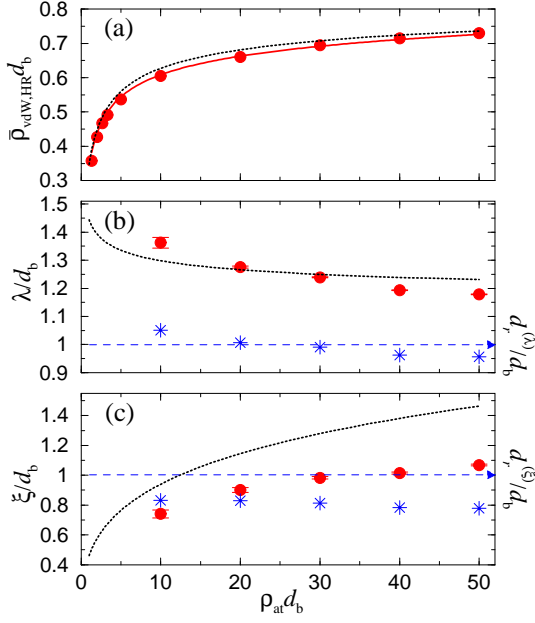


FIG. 4. (a) Average density $\bar{\rho}_{\text{vdW}} = \rho_{\text{at}} \bar{\sigma}_{rr}$ of Rydberg excitations of vdW interacting atoms vs. the atom density ρ_{at} obtained from MC simulations (circles) and Eq. (6) (solid red line). Also shown the average excitation density $\bar{\rho}_{\text{HR}}$ of Eq. (10) for the HR potential of range $d_r = d_b$ (dotted black line). (b) Oscillation period λ and (c) decay length ξ of spatial correlations of excitations $g^{(2)}(x)$ vs. the atom density ρ_{at} . For vdW interaction potential, the data points (red circles with uncertainty) are extracted from the MC simulations; for HR potential, λ and ξ are obtained from the solution of Eq. (15). The effective range $d_r^{(\lambda, \xi)}$ (blue stars: right vertical axes) of the HR potential is obtained by equating λ (b) and ξ (c) for the vdW and HR interactions.

A. Rate equations model

In [27] we have introduced a rate equations treatment of the 1D system with complete blockade of Rydberg excitations of neighboring atoms. We now extend this formalism to the longer-range interatomic interactions. To this end, we consider N atoms on a lattice, with one atom per site, and assume that the atoms excited to the Rydberg state $|r\rangle$ interact via the HR potential of range d_r : $\Delta(\mathbf{x}_i - \mathbf{x}_j) = C_\infty \Theta(|\mathbf{x}_i - \mathbf{x}_j| - d_r)$ with $C_\infty \gg w$ and $\Theta(x)$ being the step function. An atom in state $|r\rangle$ blocks the excitation of $N_r = \rho_{\text{at}} d_r$ neighboring atoms on both sides along the chain. For each atom, we then have two incoherent processes: a pump from $|g\rangle$ to $|r\rangle$ with rate P , conditioned upon the absence of Rydberg excitations within the range d_r , $\hat{L}_p^j = \sqrt{P} \hat{\sigma}_{rg}^j \prod_{|x_i - x_j| \leq d_r} (\hat{\sigma}_{rr}^i - \mathbf{1})$; and a deexcitation from $|r\rangle$ to $|g\rangle$ with rate D , $\hat{L}_d^j = \sqrt{D} \hat{\sigma}_{gr}^j$. The ratio of the two rates $\kappa \equiv \frac{P}{D} = \frac{\langle \hat{\sigma}_{rr} \rangle}{1 - \langle \hat{\sigma}_{rr} \rangle}$ is obtained from Eqs. (2) with $\delta = 0$ as

$$\kappa = \frac{|\Omega|^2}{|\Omega|^2 + \frac{1}{2} \Gamma_r \gamma_{rg}}. \quad (7)$$

The density operator of the system obeys the equation of motion

$$\partial_t \hat{\rho} = \sum_j (2\hat{L}_p^j \hat{\rho} \hat{L}_p^{j\dagger} - \{\hat{L}_p^{j\dagger} \hat{L}_p^j, \hat{\rho}\} + 2\hat{L}_d^j \hat{\rho} \hat{L}_d^{j\dagger} - \{\hat{L}_d^{j\dagger} \hat{L}_d^j, \hat{\rho}\}). \quad (8)$$

After sufficient relaxation time, the density matrix attains a classical form $\hat{\rho} = \sum_{\{\mu_j\}} p(\{\mu_j\}) |\{\mu_j\}\rangle \langle \{\mu_j\}|$, where $p(\{\mu_j\})$ is the probability of the N -atom configuration $\{\mu_j\} \in (g, r)^N$. In the steady state of the system, we have the detailed balance relations

$$\frac{p(\{\mu_j\})}{p(\{\mu'_j\})} = \kappa^{M - M'}, \quad (9)$$

where $M \equiv \langle \{\mu_j\} | \sum_j \hat{\sigma}_{rr}^j | \{\mu_j\} \rangle$ is the total number of excitations in $\{\mu_j\}$. States with the same number of excitations have equal weight and the partition function is given by $Z_N = \sum_{M=0}^N \Lambda(M, N) \kappa^M$, where $\Lambda(M, N) = \binom{N - N_r(M-1)}{M}$ is the number of possible arrangements of M excitations on a lattice of N sites, with any two excitations separated by at least N_r sites. The mean number of excitation is given by $\bar{M} = \frac{1}{Z_N} \sum_{M=0}^N \Lambda(M, N) \kappa^M$ while the average (background) density is $\bar{\rho}_{\text{HR}} = \bar{M}/N$. In a large system $N \gg N_r$, $\Lambda(M, N) \kappa^M$ is a highly peaked function of M ; finding its maximum at $M_{\text{max}} \simeq \bar{M}$ we obtain the density

$$\bar{\rho}_{\text{HR}} = \frac{1}{d_r} \frac{W(\beta)}{1 + W(\beta)}, \quad (10)$$

where $\beta = \kappa N_r$ and $W(\beta)$ is the Lambert function defined via $W e^W = \beta$. For $\beta \gg 1$, the density approaches $\bar{\rho}_{\text{HR}} \rightarrow 1/d_r$. We note that Eq. (10) is also obtained in the classical model of hard rods [35] where d_r is the rod length and β is a free parameter. Our derivation, however, yields

$$\beta = \kappa \rho_{\text{at}} d_r, \quad (11)$$

which is uniquely determined through the system parameters.

Next to the boundary at $x = 0$, the density of excitations reads

$$\rho_{\text{HR}}(x) = \frac{W(\beta) e^{-W(\beta)x/d_r}}{d_r} \sum_{k=0}^{\infty} \Theta(x/d_r - k) \frac{\beta^k (x/d_r - k)^k}{k!}, \quad (12)$$

and the spatial correlations are given by $g^{(2)}(x) = \rho_{\text{HR}}(x - d_r)/\bar{\rho}_{\text{HR}}$. At distances $x > d_r$, the correlations have the form of decaying spatial oscillations

$$g^{(2)}(x) \simeq 1 + A \cos(2\pi x/\lambda + \phi) e^{-x/\xi}, \quad (13)$$

where the oscillation period and decay length,

$$\lambda = d_r \frac{2\pi}{b}, \quad (14a)$$

$$\xi = d_r \ln^{-1} \left(\frac{-b}{W(\beta) \sin(b)} \right), \quad (14b)$$

are determined by the solution of the transcendental equation for b ,

$$\ln(W(\beta)) + W(\beta) - \ln\left(\frac{-b}{\sin(b)}\right) + \frac{b}{\tan(b)} = 0. \quad (15)$$

B. Comparison of the vdW and HR potentials

To quantify the suitability of the HR model [21] for the description of the system under the vdW potential, we now compare the mean densities of excitations $\bar{\rho}_{\text{vdW,HR}}$, as well as the oscillation periods λ and decay lengths ξ of spatial correlations $g^{(2)}(x)$.

Let us first equate the range of the HD potential to the blockade distance of the vdW potential, $d_r = d_b$. The average densities of excitations are then remarkably close, $\bar{\rho}_{\text{vdW}} \simeq \bar{\rho}_{\text{HR}}$, especially at high atomic densities $\rho_{\text{at}} d_b \gg 1$, see Fig. 4(a). With increasing the atomic density, however, the oscillation period λ of the density wave decreases faster for the vdW potential, Fig. 4(b); apparently the superatoms having soft boundaries can pack closer to each other. The same softness of the vdW potential, compared to the HR potential, can explain shorter correlation lengths ξ , see Fig. 4(c).

Next, we may assume equal oscillation periods λ for both potentials and then deduce the corresponding range $d_r^{(\lambda)}$ of the HR potential, which turns out to be close to d_b but slowly decreasing with increasing the atomic density ρ_{at} , Fig. 4(b). Alternatively, we equate the correlation lengths ξ and find somewhat smaller corresponding range of the HR potential, $d_r^{(\xi)} \simeq 0.8d_b$, again slowly decreasing with increasing the atomic density ρ_{at} , Fig. 4(c).

Finally, we have performed MC simulations for $N \gg 1$ strongly-driven atoms interacting via the HR potential. In Fig. 5 we compare the the correlation functions $g^{(2)}(x)$ obtained from our simulations and the corresponding analytic solutions with the results for the vdW interacting atoms under the otherwise identical conditions. We observe qualitatively similar behavior when the range d_r of the HR potential is equal to the blockade distance d_b of the vdW potential. Alternatively [21], we may associate the range of the HR potential d_r with the collective blockade distance d_{cb} in which case $\beta = \kappa N_{\text{cb}} = \kappa(\rho_{\text{at}} d_b)^{12/13}$. As seen in the insets of Figs. 5, the correlation functions for vdW and HR potentials are now considerably different, the corresponding oscillation periods being an approximately constant $\lambda \simeq 1.75d_{\text{cb}}$ for the vdW potential, and a slowly varying $\lambda \simeq 1.3 - 1.25d_{\text{cb}}$ for the HR potential.

V. CONCLUDING REMARKS

The system studied in this paper corresponds to an ensemble of cold alkali atoms excited to the strongly-interacting Rydberg states $|r\rangle$ with principal quantum number $n \sim 50 - 100$. The resonant atomic excitation

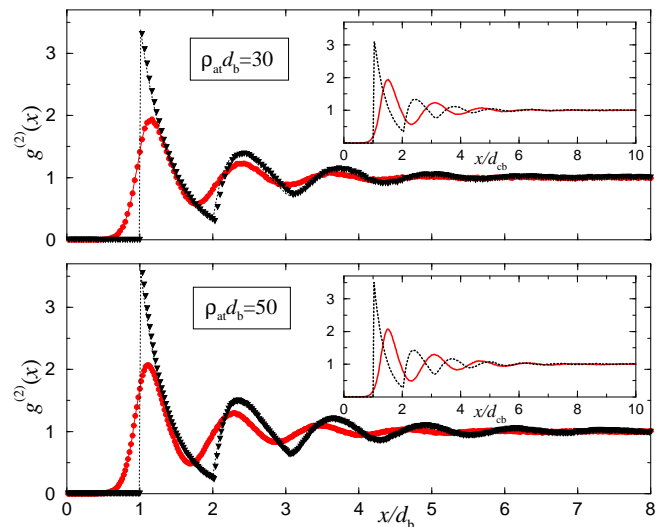


FIG. 5. Correlations $g^{(2)}(x)$ of atomic excitations for vdW (circles) and HR (triangles) potentials obtained from MC simulations with atom densities $\rho_{\text{at}} d_b = 30$ (top) and $\rho_{\text{at}} d_b = 50$ (bottom). In the insets, $g^{(2)}(x)$ are plotted versus x in units of the collective blockade distance d_{cb} . Atomic parameters are as in Fig. 3.

is effected by either direct one-photon (UV) transition $|g\rangle \rightarrow |r\rangle$ or two-photon transition via non-resonant intermediate state [25]. Typical values for the driving field Rabi frequency $\Omega \sim 10^5$ Hz, together with the relaxation rates $\Gamma_r \lesssim 0.1\Omega$ and $\gamma_{rg} \simeq 2\Omega$, lead to the blockade distance in the range of $d_b \sim 5 - 10 \mu\text{m}$. The low-density ensemble of equidistant atoms is trapped in a 1D optical lattice. At higher densities, regular arrangement of atoms in a lattice would play a minor role and our results should hold also in the continuous gas of atoms confined in an elongated trap with transverse dimension much smaller than the blockade distance.

To summarize, we have shown that the steady-state probabilities of Rydberg excitations in resonantly-driven atomic ensembles can exhibit damped spatial oscillations and quasi-crystallization due to the strong interactions between the atomic Rydberg states. The inverse wavelength and correlation length of these oscillations grow with the probability of collective Rydberg excitations of superatoms which increases with the atomic density and thereby the cooperativity of the excitations. An analytic model based on a “hard-rod” interatomic potential can serve as a guide to understanding the properties of the system under the van der Waals potential.

After sudden switching-off of the driving field, the Rydberg quasi-crystal can survive for tens or hundreds of microseconds, it can be detected *in situ* by spatially-resolved Rydberg state ionization [23] or high-resolution fluorescence imaging [24].

ACKNOWLEDGMENTS

Financial support of the DFG through SFB TR49 is acknowledged. D.P. is grateful to the University of Kaiserslautern for hospitality and support.

-
- [1] T.F. Gallagher, *Rydberg Atoms* (Cambridge University Press, Cambridge, 1994).
- [2] M.D. Lukin, M. Fleischhauer, R. Côté, L.M. Duan, D. Jaksch, J.I. Cirac, and P. Zoller, Phys. Rev. Lett. **87**, 037901 (2001).
- [3] D. Tong, S.M. Farooqi, J. Stanojevic, S. Krishnan, Y.P. Zhang, R. Côté, E.E. Eyler, and P.L. Gould, Phys. Rev. Lett. **93**, 063001 (2004).
- [4] K. Singer, M. Reetz-Lamour, T. Amthor, L.G. Marcassa, and M. Weidemüller, Phys. Rev. Lett. **93**, 163001 (2004).
- [5] T. Vogt, M. Viteau, J. Zhao, A. Chotia, D. Comparat, and P. Pillet, Phys. Rev. Lett. **97**, 083003 (2006).
- [6] R. Heidemann, U. Raitzsch, V. Bendkowsky, B. Butscher, R. Löw, L. Santos, and T. Pfau, Phys. Rev. Lett. **99**, 163601 (2007).
- [7] E. Urban, T.A. Johnson, T. Henage, L. Isenhower, D.D. Yavuz, T.G. Walker, and M. Saffman, Nature Phys. **5**, 110 (2009); A. Gaëtan, Y. Miroshnychenko, T. Wilk, A. Chotia, M. Viteau, D. Comparat, P. Pillet, A. Browaeys, and P. Grangier, *ibid* **5**, 115 (2009).
- [8] Y.O. Dudin, L. Li, F. Bariani, and A. Kuzmich, Nature Phys. **8**, 790 (2012).
- [9] M. Saffman, T.G. Walker, and K. Mølmer, Rev. Mod. Phys. **82**, 2313 (2010).
- [10] H. Weimer, R. Löw, T. Pfau, and H.P. Büchler, Phys. Rev. Lett. **101**, 250601 (2008).
- [11] R. Löw, H. Weimer, U. Krohn, R. Heidemann, V. Bendkowsky, B. Butscher, H.P. Büchler, and T. Pfau, Phys. Rev. A **80**, 033422 (2009).
- [12] H. Weimer and H.P. Büchler, Phys. Rev. Lett. **105**, 230403 (2010).
- [13] J. Schachenmayer, I. Lesanovsky, A. Micheli, and A.J. Daley, New J. Phys. **12**, 103044 (2010).
- [14] I. Lesanovsky, Phys. Rev. Lett. **106**, 025301 (2011).
- [15] E. Sela, M. Punk, and M. Garst, Phys. Rev. B **84**, 085434 (2011).
- [16] T. Pohl, E. Demler, and M.D. Lukin, Phys. Rev. Lett. **104**, 043002 (2010).
- [17] R.M.W. van Bijnen, S. Smit, K.A.H. van Leeuwen, E.J.D. Vredenburg, and S.J.J.M.F. Kokkelmans, J. Phys. B **44**, 184008 (2011).
- [18] G. Pupillo, A. Micheli, M. Boninsegni, I. Lesanovsky, and P. Zoller, Phys. Rev. Lett. **104**, 223002 (2010).
- [19] S. Ji, C. Ates and I. Lesanovsky, Phys. Rev. Lett. **107**, 060406 (2011).
- [20] I. Lesanovsky, Phys. Rev. Lett. **108**, 105301 (2012).
- [21] C. Ates and I. Lesanovsky, Phys. Rev. A **86**, 013408 (2012).
- [22] M. Viteau, M.G. Bason, J. Radogostowicz, N. Malossi, D. Ciampini, O. Morsch, E. Arimondo, Phys. Rev. Lett. **107**, 060402 (2011).
- [23] A. Schwarzkopf, R.E. Sapiro, and G. Raithel, Phys. Rev. Lett. **107**, 103001 (2011).
- [24] P. Schauf, M. Cheneau, M. Endres, T. Fukuhara, S. Hild, A. Omran, T. Pohl, C. Gross, S. Kuhr, and I. Bloch, Nature **491**, 87 (2012).
- [25] R. Löw, H. Weimer, J. Nipper, J.B. Balewski, B. Butscher, H.P. Büchler, and T. Pfau, J. Phys. B **45**, 113001 (2012).
- [26] M. Gärttner, K.P. Heeg, T. Gasenzer and J. Evers, arXiv:1203.2884.
- [27] M. Hoening, D. Muth, D. Petrosyan, and M. Fleischhauer, arXiv:1208.2911.
- [28] F. Robicheaux and J.V. Hernandez, Phys. Rev. A **72**, 063403 (2005).
- [29] J. Stanojevic and R. Côté, Phys. Rev. A **80**, 033418 (2009).
- [30] J. Honer, R. Löw, H. Weimer, T. Pfau, and H.P. Büchler, Phys. Rev. Lett. **107**, 093601 (2011).
- [31] We assume the static DD interaction between the atoms in Rydberg states possessing permanent dipole moments induced by an external dc electric field [1].
- [32] C. Boisseau, I. Simbotin, and R. Côté, Phys. Rev. Lett. **88**, 133004 (2002); K. Singer, J. Stanojevic, M. Weidemüller, and R. Côté, J. Phys. B **38**, S295 (2005).
- [33] P. Lambropoulos and D. Petrosyan, *Fundamentals of Quantum Optics and Quantum Information*, (Springer, Berlin, 2007) Chap. 4.
- [34] K.P. Heeg, M. Gärttner and J. Evers, arXiv:1202.2779.
- [35] Z.W. Salsburg, R.W. Zwanzig, and J.G. Kirkwood, J. Chem. Phys. **21**, 1098 (1953); A. Robledo and J. S. Rowlinson, Molec. Phys. **58**, 711-721 (1986).